

PAPER


## Gray: a ray tracing-based Monte Carlo simulator for PET

To cite this article: David L Freese *et al* 2018 *Phys. Med. Biol.* **63** 105019

View the [article online](#) for updates and enhancements.

### Related content

- [Validation of the SimSET simulation package for modeling the Siemens Biograph mCT PET scanner](#)  
Jonathan K Poon, Magnus L Dahlbom, Michael E Casey *et al.*
- [Monte Carlo simulations versus experimental measurements in a small animal PET system. A comparison in the NEMA NU 4-2008 framework](#)  
F D Popota, P Aguiar, S España *et al.*
- [GATE Monte Carlo simulations for variations of an integrated PET/MR hybrid imaging system based on the Biograph mMR model](#)  
B Aklan, B W Jakoby, C C Watson *et al.*



**Explore the latest innovations  
in radiation therapy QA**

Meet Modus QA at **AAPM Virtual Annual Meeting**  
July 25 - 29, 2021

**MODUS QA**



## PAPER

## Gray: a ray tracing-based Monte Carlo simulator for PET

RECEIVED  
20 January 2018REVISED  
20 April 2018ACCEPTED FOR PUBLICATION  
27 April 2018PUBLISHED  
21 May 2018David L Freese<sup>1</sup>, Peter D Olcott<sup>2</sup>, Samuel R Buss<sup>3</sup> and Craig S Levin<sup>1,4</sup><sup>1</sup> Department of Electrical Engineering, Stanford University, Stanford, CA, United States of America<sup>2</sup> RefleXion Medical, Hayward, CA, United States of America<sup>3</sup> Department of Mathematics at the University of California, San Diego, CA, United States of America<sup>4</sup> Departments of Radiology, Physics, and Bioengineering, Stanford University, Stanford, CA, United States of AmericaE-mail: [cslevin@stanford.edu](mailto:cslevin@stanford.edu)

Keywords: PET, simulation, Monte Carlo, open source, NEMA

**Abstract**

Monte Carlo simulation software plays a critical role in PET system design. Performing complex, repeated Monte Carlo simulations can be computationally prohibitive, as even a single simulation can require a large amount of time and a computing cluster to complete. Here we introduce Gray, a Monte Carlo simulation software for PET systems. Gray exploits ray tracing methods used in the computer graphics community to greatly accelerate simulations of PET systems with complex geometries. We demonstrate the implementation of models for positron range, annihilation acolinearity, photoelectric absorption, Compton scatter, and Rayleigh scatter. For validation, we simulate the GATE PET benchmark, and compare energy, distribution of hits, coincidences, and run time. We show a  $13.6 \pm 0.1 \times$  speedup using Gray, compared to GATE for the same simulation, while demonstrating nearly identical results. We additionally simulate the Siemens Biograph mCT system with both the NEMA NU-2 scatter phantom and sensitivity phantom. We estimate the total sensitivity within  $3 \pm 2\%$  when accounting for differences in peak NECR. We also estimate the peak NECR to be  $199.5 \pm 0.2$  kcps, or within  $0.5 \pm 0.1\%$  of published experimental data. The activity concentration of the peak is also estimated within 1.3%.

**1. Introduction**

Monte Carlo simulations are of great use for PET system development as they allow different system designs to be explored without expensive construction or testing. This, however, requires accurate modeling of the physics of PET systems. This can be a computationally expensive task, as the propagation of high-energy photons must be tracked through complex geometries, and their interactions with these materials must be modeled accurately. Designing a Monte Carlo simulation that is both accurate and fast requires making important choices about what physical effects to model and how to do so efficiently.

Two of the most commonly used software packages for Monte Carlo simulations of PET are GATE and SimSET (Harrison *et al* 2006). GATE is the most comprehensive piece of software for modeling PET systems (Jan *et al* 2011). Based on Geant4, a physics library published by CERN, it is able to accurately model the physics of photon transport through various materials (e.g. in the patient and the detector system), as well as the various methods through which energy is deposited into detector materials, such as scintillation crystals. Depending on the needs of the user, different physical phenomenon can be enabled or disabled to accelerate the simulation, or make it more accurate. GATE is, however, traditionally known for being quite computationally expensive. GATE also contains tools to model the electronics chains present in PET systems, which allows for reduction of the data output from the simulation (Guez *et al* 2008). This is important as the number of hits required to simulate even a small number of coincidence events can be prohibitively large. It is also important, as the readout electronics can play an important factor in the imaging quality and count rate performance of a system.

SimSET is a public-domain software package that was designed to model both SPECT and PET systems (Harrison *et al* 1993). From its initial inception it has been developed to model photoelectric absorption, Compton Scatter, Rayleigh Scatter (Kaplan *et al* 1998), positron annihilation acolinearity (Harrison *et al* 1999), and block detectors (Harrison *et al* 2006). Its design is primarily based around cylindrical geometries, so it does limit

the types of systems that can be simulated. Detectors have some requirements of rotational symmetry, and the activity distribution simulated is limited to inside the cylinder circumscribed by the detectors. Furthermore, SimSET does not support simulation of the readout electronics.

Both GATE and SimSET have been shown to produce results that correlate well with experimental data. Particularly, both packages demonstrate accurate modeling of the experimental results from PET scanners under standardized NEMA NU-2 measurements (Lamare *et al* 2006, Schmidlein *et al* 2006, Gonias *et al* 2007, MacDonald *et al* 2008, Delso *et al* 2011, Poon *et al* 2012, 2015, Aklan *et al* 2015).

GATE models the physics within a PET system, in part, by stepping through the geometry and testing for interactions at each step. However, if one makes the assumption that a photon will travel straight until it interacts with a material, then it becomes quite natural to borrow from the concept of ray tracing, which is used in the field of animation and computer graphics to render complex scenes in great detail. This allows the full distance of travel of a particle in a volume to be calculated. The probability of a particular interaction and its location can then be estimated from the distance of travel. This method reduces the number of steps through the geometry required per photon to the number of unique volumes through which the photon travels.

Here we will introduce a new Monte Carlo simulation tool, called Gray, short for gamma ray tracer, publicly released under the MIT open source license. We will explain the methods and assumptions behind the ray tracing, physics, and data acquisition models contained within Gray, and then run several simulations to both validate the proper implementation of these models, as well as compare the results with GATE on well established benchmarks. We also simulate the Siemens Biograph mCT with the NEMA NU2-2007 scatter phantom and sensitivity phantom and compare the results to published experimental results.

## 2. Methods

### 2.1. Raytracing

Gray uses a ray tracing program adapted from the example published by Buss (2003). This program provides a basis for calculating the intersection of a ray with a variety of different viewable shape objects. The foundation of this program is a k-d tree data structure. K-d trees are an efficient data structure for segmenting N-dimensional space so that a nearest point can be found efficiently. The k-d tree in this case is combined with an axis-aligned bounding box (AABB) to quickly find the extents of an object, and then test for a possible intersection. If a possible intersection does exist, a function specific to the viewable object type is used to test for an actual intersection and the intersection distance. This intersection distance is then used within physics models to calculate interaction probabilities.

Each of the objects within a simulation is stored on a leaf of the k-d tree. The leaves are sorted under nodes of the k-d tree which contain information on how to split the scene along an X, Y, or Z-aligned plane. Nodes are nested under other nodes to form a tree structure, which is traversed to move about the scene. As the program visits a leaf, it checks for an intersection between the ray along which the photon is traveling and the objects in that leaf. For most scenes, a k-d tree requires traversing an average of  $O(\log n)$  nodes before reaching a leaf, where  $n$  is the number of viewable objects in the scene. Assuming a photon requires a constant number of traversal calculations, our simulation then scales as  $O(m \log n)$ , where  $m$  is the number of photons we must simulate.

Gray supports a number of basic shapes, such as spheres, cylinders, rectangular prisms, that can be used as detectors, sources, or neither. All of these geometries for a simulation can be viewed using an OpenGL-based viewer included in Gray, depicted in figure 1. One primary benefit of Gray's foundation on a ray tracing model is that any arbitrary geometry can be modeled as a collection of polygons. The number of polygons is limited only by the memory needed to store the polygons and the K-d tree. This allows for complex phantoms, such as a person or mouse, to be easily modeled. These phantoms can then also be used as a source or a detector. When used as a source, the volume is surrounded by an AABB. A decay is then randomly generated within the bounds of the AABB, and a ray is cast from that point to make sure the interior of the material is intersected, as shown in figure 2. In this way, almost any three-dimensional model of an object could be turned into a source.

### 2.2. Physics

Gray currently models five physical properties dominant in PET imaging: positron range, annihilation acolinearity, photoelectric absorption, Compton scatter, and Rayleigh scatter. For positron range, we primarily use the double exponential model introduced by Derenzo (1979), and simulated for multiple isotopes by Levin and Hoffman (1999).

$$P(x) = aCe^{k_1x} + a(1 - C)e^{k_2x} \quad (1)$$

$$a = \left[ 1 + \frac{k_1}{k_2} \left( \frac{1}{C} - 1 \right) \right]^{-1}. \quad (2)$$

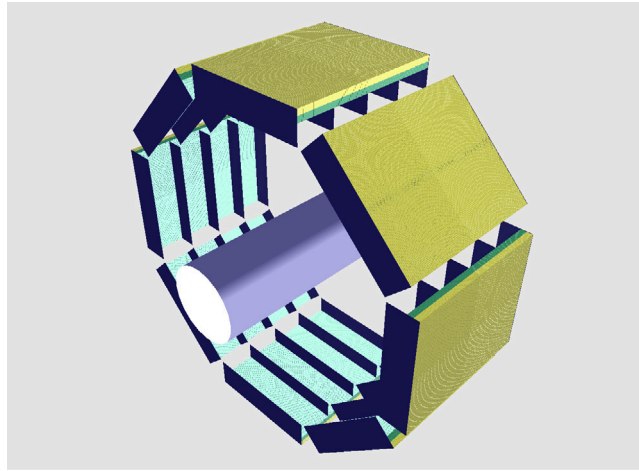


**Figure 1.** Gray includes an OpenGL-based viewer so that geometries can be visualized in 3D. Shown here is the GATE PET benchmark simulation (Jan *et al* 2011). The BGO and LSO crystals are shown in yellow and blue, respectively. The cylindrical phantom is seen in the center, with the tungsten septa and lead shielding in dark blue.

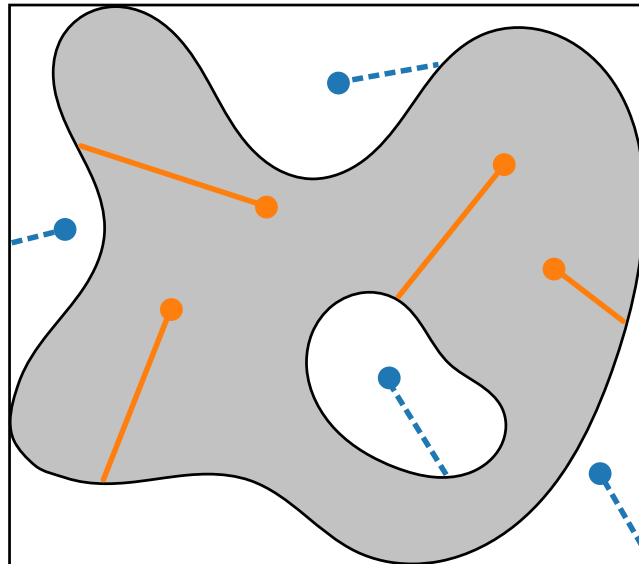


**Figure 2.** Arbitrary source geometries, such as a heart or a lung, can be modeled using a polygon mesh. Positrons are randomly generated inside of the object's enclosing AABB. A ray is cast from the position to determine whether or not it is inside of the active geometry. The ray tracing software provides a mechanism to detect whether the inside or outside of an object was detected. We label rejected positrons with blue dashed lines and accepted ones with solid orange lines.

We have introduced the parameter  $a$  to scale  $P(x)$  so it can be used as a probability density function. The parameter  $C$  controls the mix between the two exponential models. This model currently assumes a uniform material, for which water is used as a default. Gray is able to load in any user defined isotope, where its half-life, branching ratio (probability of emitting a positron), prompt gamma emission (if any), and positron range are defined. This allows positron range to be modified for other materials. The next three properties, photoelectric absorption, Compton scatter, and Rayleigh scatter use the Evaluated Photon Data Library (EPDL), commonly known as the Livermore model (Cullen *et al* 1997). A material's chemical composition and density are used to calculate probabilities of Compton scattering or photoelectric absorption across a variety of energies relevant for PET, making sure that K-edge absorption discontinuities are taken into account. Log-log interpolation is performed between distinct energies to calculate the linear attenuation coefficient, and thus the probability of interaction in an object.

For the scattered angle and deposited energy, the Klein–Nishina model, modified by the scattering function in the EPDL is used. The Livermore model defines the differential cross section for Compton Scattering as follows:

$$\frac{\delta\sigma_c}{\delta\Omega} = S(x) \frac{\delta\sigma_{kn}}{\delta\Omega} \quad (3)$$

where  $S$  is the scattering function tabulated in the EPDL. The scattering parameter,  $x$ , and the Klein–Nishina differential cross section,  $\frac{\delta\sigma_{kn}}{\delta\Omega}$  are defined by:

$$x(\theta, E) = \frac{E}{hc} \sin\left(\frac{\theta}{2}\right) \quad (4)$$

$$\frac{\delta\sigma_{kn}}{\delta\Omega} = \frac{r_c^2}{2} P \left( P + \frac{1}{P} + \sin^2\theta \right) \quad (5)$$

where  $E$  is the incoming photon energy and  $\theta$  is the scattering angle. The constant  $r_c$  is the classical electron radius, and  $h$  and  $c$  are Planck's constant and the speed of light, respectively. The parameter  $P$  is defined in terms of scattering angle and energy of the incoming photon. The variable  $\alpha$  is the ratio of the incident photon energy to the rest mass of an electron.

$$P(\theta, E) = (1 + \alpha(1 - \cos\theta))^{-1}. \quad (6)$$

A similar form is used for the differential cross section of Rayleigh scattering,  $\frac{\delta\sigma_r}{\delta\Omega}$ , by modifying the classical Thompson differential cross section,  $\frac{\delta\sigma_t}{\delta\Omega}$ , by the scattering form factor,  $F(x)$ .

$$\frac{\delta\sigma_r}{\delta\Omega} = F(x)^2 \frac{\delta\sigma_t}{\delta\Omega} \quad (7)$$

$$\frac{\delta\sigma_t}{\delta\Omega} = \frac{r_c^2}{2} (1 + \cos^2\theta). \quad (8)$$

$F(x)$ , like  $S(x)$ , is also tabulated in the EPDL. Each of the differential cross sections are then integrated in the azimuthal angle  $\phi$ , and converted into cumulative distribution function in terms of the radial angle,  $\theta$ . A unique cumulative distribution function is created for every material specified, from which the inversion method is used to generate a random angle. Acolinearity is, by default, modeled as a  $0.57^\circ$  full-width at half-max (FWHM) Gaussian deviation from a perfect  $180^\circ$ , back-to-back annihilation (Shibuya *et al* 2007). Acolinearity, however, can be disabled or modified by the user on a per-isotope basis. Gray does not currently take into account three-photon positron annihilation, as this occurs 1/137 of the time (Ore and Powell 1949, DeBenedetti and Siegel 1954).

### 2.3. DAQ model

We have modeled the data acquisition (DAQ) system for Gray as a series of processes that operate on the energy depositing interactions, or 'hits', calculated by the physics model of Gray. Each process takes in a set of hits, performs a particular operation that could potentially modify the hit, and returns the result. This set of hits is then passed to the next process until the entire process chain is complete. The resulting output of the process chain is referred to as singles events. The singles events are then typically passed to two coincidence processors that will sort out coincidence events. Two coincidence processors allows for a delay window correction scheme to be implemented. For the singles process chain, the different process types that are supported are filtering, blurring, dead time, and merging.

Filtering allows energy discrimination to be performed on the stream. A blurring process will blur either the time or energy of the pulse with a Gaussian distribution of a specified width. The energy blurring process is allowed to either be a fixed percentage of the current energy, or to degrade with the inverse square of energy compared to a reference energy. A dead time process will remove events from the stream based on either a paralyzable or a non-paralyzable model. Finally, the merging process will combine hits together, taking into account energy and position. For the dead time and merging processes, the structure of the system can be taken into account by mapping each detector element in the system to a particular component, such as a block detector or readout chip. By specifying that all detectors belong to the same detector block, hits within that block could be merged together using Anger logic, for example.

The coincidence processors operate in parallel on the singles output. These processors tag each of the singles events in a coincidence event as having the same coincidence ID. Multiples events, where more than two singles occur within the same coincidence window, can optionally be kept or rejected.

The Gray DAQ model operates independently of the physics model of Gray. This allows for a stand alone application that takes in hits, or singles, and is able to run the exact same data acquisition model, similar to DigiGATE (Jan *et al* 2011). This makes it an incredibly useful tool for exploring system design choices, such as multiplexing, that can have complicated and adverse effects on system performance, while keeping the geometry and physics constant. An advantage over DigiGATE is that the standalone Gray DAQ model is able to work with hits or singles data, allowing data output to be reduced significantly compared to hits alone. This feature allows the DAQ model to be terminated and restarted after any process step, allowing for parameters of a particular process to be explored efficiently.



## 2.4. Parallelism

Monte Carlo simulations of PET systems lend themselves well to parallel computing environments, as the simulation can easily be split in time across many computing nodes to reducing the total time required for the simulation. To take advantage of this property, we have implemented native multithread support in Gray. The simulation is split up across threads based on time. Half lives and decay properties of different isotopes from sources in the simulation are accounted for so the work is evenly distributed across all nodes. We do not bridge the data acquisition model across the splits in the file, as we regard this as a minor effect.

## 2.5. Model validation

We perform three different simulations to validate that Gray accurately models the physical properties within a PET system. First we model a point source of  $^{18}\text{F}$  inside of water and log the annihilation positions of the positrons. The distribution of annihilation points is then compared to the Monte Carlo results presented by Levin and Hoffman (1999).

Next we model a mono-energy (511 keV), pencil beam source aimed at a large (100 cm  $\times$  100 cm  $\times$  100 cm) block of LSO ( $\text{Lu}_2\text{SiO}_5$ , density = 7.4 g ml $^{-1}$ ,  $Z_{\text{eff}} = 56.5$ ). We place a second block of the same size behind the source to catch backscattered radiation. We log the first position of interaction for the photon and compare this to the model predicted by XCOM for that material type. Additionally for Compton scatter events, the scattering angle is calculated and compared to the model predicted by Klein–Nishina.

For the last simulation, we run the GATE PET Benchmark in both GATE and Gray. The geometry of the benchmark can be seen in figure 1. The GATE PET benchmark is a simulation with 1280 000 crystals (half BGO, half LSO), tungsten septa, lead end shielding, and a cylindrical phantom containing two sources with 100 kBq of  $^{15}\text{O}$  and  $^{18}\text{F}$ , respectively. The resulting energy spectra, spatial distribution of hits and coincidences, and runtime is compared. We examine the statistical relevance of these differences compared to the standard deviation of a Poisson random variable with a mean of the GATE simulation value. We contextualize the magnitude of this difference by running a second benchmark simulation in GATE and performing the same analysis as was done for Gray. For these simulations, we disable motion of the scanner within GATE. To compare runtime, we run each simulation 3 times and report mean and standard error for both GATE and Gray. For both GATE and Gray we additionally report the percentage of the total runtime required to simulate the hits in the system without output or a DAQ model. We also use the GATE PET Benchmark to demonstrate Gray's multithreading capabilities. We run Gray using 1 up to 8 threads on an quad-core Intel i7 and report the speed-up in simulation time relative to the single thread case. Finally, we report the percentage of runtime required for GATE to complete the benchmark with the positron sources in the benchmark replaced with a geantino particle source. The geantino is a fictional particle that does not interact with any materials. We do this simulation to contextualize the amount of processing time that is spent tracking annihilation photons through the simulated world. The source activity is doubled for the geantino source to make sure the number of geantinos matches the number of photons from positron annihilation.

## 2.6. Simulation of a clinical PET system

Following the procedures outlined by Poon *et al*, we simulate the Siemens mCT PET/CT scanner with the NEMA NU-2 2007 scatter phantom (Poon *et al* 2012, 2015). The Siemens scanner has a PET system with a ring diameter of 84.9 cm. The system's 192 blocks of crystal arrays (4 axially and 48 transaxially) contain a square array of 169 LSO crystals, each measuring 4 mm by 4 mm by 20 mm. The cover of the scanner is modeled as plastic, and the patient bed as carbon fiber. We do not model the  $^{176}\text{Lu}$  background in the LSO of the scanner. A set of blocks 4 wide axially, and 1 radially are tied together into what is termed a bucket. Two buckets radially are then multiplexed together and are allowed one single event per system clock cycle of 80 ns. Only the first event is accepted in the case of many events within the two multiplexed buckets. The data acquisition (DAQ) system was modeled with the following series of processes built into Gray:

- (i) Merging of events in the same block using Anger logic if they occur within 300 ps for triggering logic.
- (ii) Gaussian energy blurring of 11.7% at 511 keV.
- (iii) Energy gating events to above 150 keV.
- (iv) Merging of events in the same block using Anger logic if they occur within 40 ns to model pulse integration.
- (v) A 40 ns non-paralyzable dead time model at the multiplexed bucket level.
- (vi) Time blurring the singles events with a Gaussian of 375.0 ps FWHM.
- (vii) Energy windowing from 435 keV to 650 keV.
- (viii) Coincidence windowing to events within 2.05 ns for a full window width of 4.1 ns, with a delayed coincidence window offset by 100 ns.

Only the parts of the DAQ that were described by Poon *et al* (2012) were put into the model. We simplify the dead time model used by Poon *et al* by using a continuous model, and neglecting the discrete behavior of the system clock. To do this, we assume the dead time will be a uniform random variable between 0 ns and 80 ns, resulting in an average dead time of 40 ns. As the exact decay time and integration time are not specified, we also assume a 40 ns integration time to match the dead time model, and do not model the exponential decay of the pulse. The maximum ring difference of 49 and minimum bucket difference of 9 specified by Poon *et al* were applied in post-processing. We additionally simplify the patient bed as a 0.6 cm thick slab of carbon fiber extending 45.0 cm transaxially and 70.0 cm axially, with 3.66 cm high rectangular sides of the same thickness and length, as Gray does not currently support the voxelized phantoms used in the GATE study.

The scatter phantom was modeled as a polyethylene cylinder 70 cm in length and 20.3 cm in diameter with a  $^{18}\text{F}$  source of the same length and 3.2 mm in diameter offset 4.5 cm below the center of the field of view. We simulate 17 activity concentration levels between  $0.38 \text{ kBq ml}^{-1}$  and  $45.1 \text{ kBq ml}^{-1}$ . We simulate 0.3 s of time for the  $45.1 \text{ kBq ml}^{-1}$  concentration. We adjust the remaining simulations for the decay of  $^{18}\text{F}$  to simulate approximately the same number of positron decays. At each activity level during the NEMA scatter phantom count rate study, a qualified singles rate per block is reported. This represents the number of events fed into the coincidence process following energy windowing. Additionally, in the same manner as Poon *et al* we report the randoms rate, trues and scatters rate, noise equivalent count rate (NECR), and scatter fraction (Poon *et al* 2012). We report an average percent difference from the experimental rate reported by Poon *et al* over all the activity concentration. We determine the experimental value for each activity concentration by linearly interpolating from the experimental data points reported. The percent difference for each point is calculated in the following manner:

$$\text{percent diff} = 100\% \left( \frac{|R_{\text{exp}} - R_{\text{sim}}|}{R_{\text{exp}}} \right) \quad (9)$$

where  $R_{\text{exp}}$  and  $R_{\text{sim}}$  are the rates from the experimental measurements by Poon *et al* (2012) and our Gray simulations, respectively. We also model the NEMA NU-2 2007 sensitivity phantom to provide a comparison to the results reported by Jakoby *et al* (2011). The sensitivity phantom was modeled as a polyethylene cylinder 70 cm in length and 3.2 mm in diameter, with a  $37.0 \text{ kBq } ^{18}\text{F}$  source. We do not simulate the aluminum sleeves specified in the NEMA standard, because the positron range model within Gray is not material dependent, so additional material is not needed to cause positron annihilation. We run the simulation 1500.0 s with the half-life of  $^{18}\text{F}$  disabled to keep a constant activity. Per the NEMA protocol described by Jakoby *et al*, we plot the axial sensitivity profile, and calculate the total sensitivity. Both Jakoby *et al* and Poon *et al* describe the same Siemens mCT system, but the peak NECR in Poon *et al* is 12% higher, and Poon *et al* does not present sensitivity numbers, so we also compare the Gray sensitivity values with those of Jakoby *et al* scaled by the difference in the peak NECR. By doing this, we assume sensitivity should scale linearly with peak NECR for the same system geometry, energy window, and time window. We report error for singles, prompts, and randoms as the estimated standard deviation of a poisson random variable. Error is propagated for all other derived quantities.

### 3. Results

The positron range distribution, compared with the model by Levin and Hoffman is shown in figure 3. The model in this figure is the probability density function (PDF) of the positron range multiplied by the number of positrons and the bin width.

In figure 4 we show the attenuation of a mono-energetic, pencil beam source into a large LSO block. For each photon, we log the position of first interaction and the type of interaction, and plot this against the linear attenuation from the Livermore model.

For photons that undergo Compton scattering, we calculate the scattering angle they undergo and the results are shown in figure 5 relative to the Livermore model. The same analysis is done for Rayleigh scattered photons in figure 6.

Next, we compare the performance of Gray on the GATE PET benchmark. When running the simulation as a single thread within a Ubuntu 14.04 virtual machine with 4GB of memory, and a single core of a 2 GHz Intel Core i7, the CPU time required was  $9.8 \pm 0.1$  min, while GATE required  $133 \pm 6$  min. The fraction of the runtime used to simulate hits within the simulation geometry was 99.6% and 92.9% for Gray and GATE, respectively. A comparison of the energy spectrum of the hits generated by each model is shown in figure 7, while the spatial distribution of hits within the crystals of the GATE benchmark can be seen in figure 8. For the spatial distribution comparison, hits within the LSO and BGO layers of the simulation are combined together.

The possible number of unique crystal pairs is quite large when comparing coincidence events. This fact makes the occurrence of any particular pair of crystals unlikely. To reduce statistical noise, we rebin the crystals in the benchmark simulation down by a factor of 100, to the module level. We then perform the same analysis for module pairs as was done for hits (figure 8), with the results shown in figure 9.

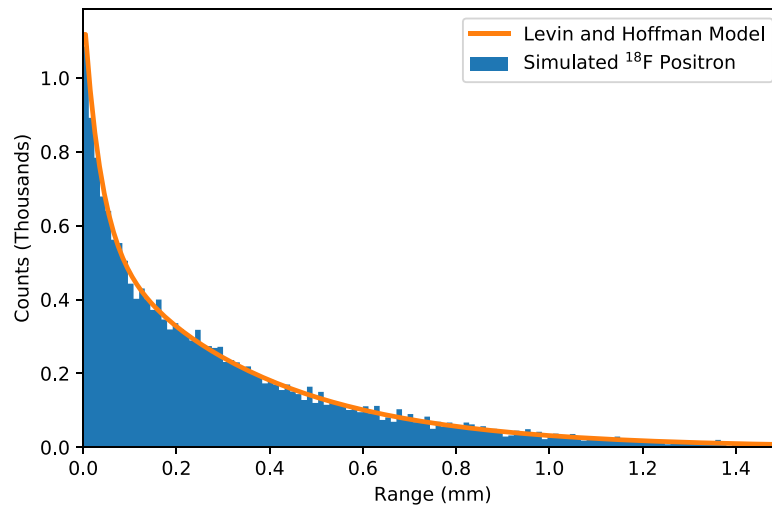


**Figure 3.** We see good agreement between the simulated positron range distribution in water, versus the analytical model proposed by Levin and Hoffman. Models for other common isotopes such as  $^{11}\text{C}$ ,  $^{13}\text{N}$ , and  $^{15}\text{O}$  have also been implemented.

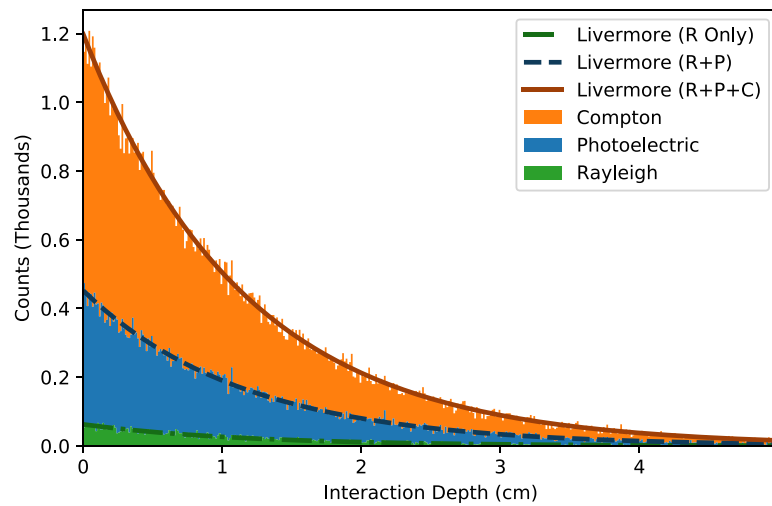


**Figure 4.** The depth of the first interaction of a 511 keV photon inside of a block of LSO is shown. The histogram is split by color to denote the proportion of photoelectric, Compton scattering, and Rayleigh scattering interactions. The Livermore-based linear attenuation model is also shown for reference.

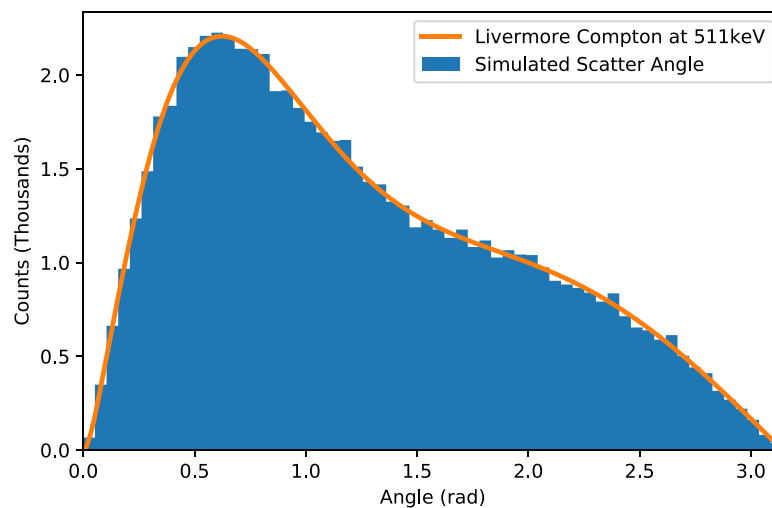


**Figure 5.** The scatter angle of all of the Compton scatter events relative to the Livermore model.



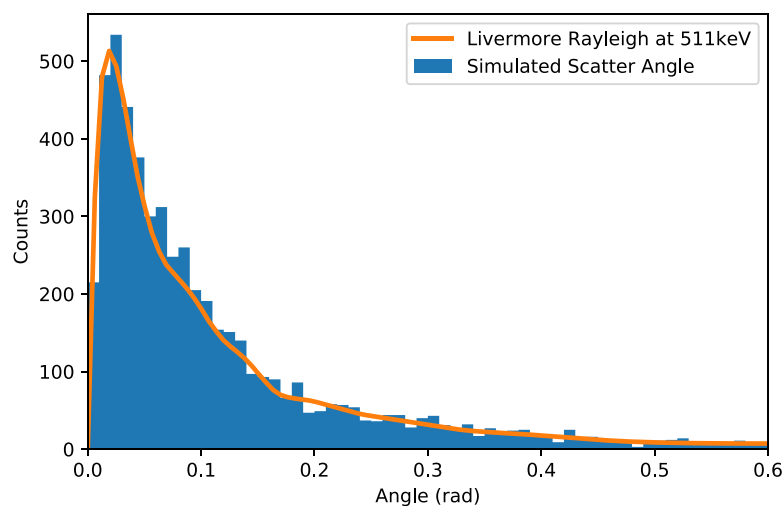


Figure 6. The scatter angle of all of the Rayleigh scatter events relative to the Livermore model.

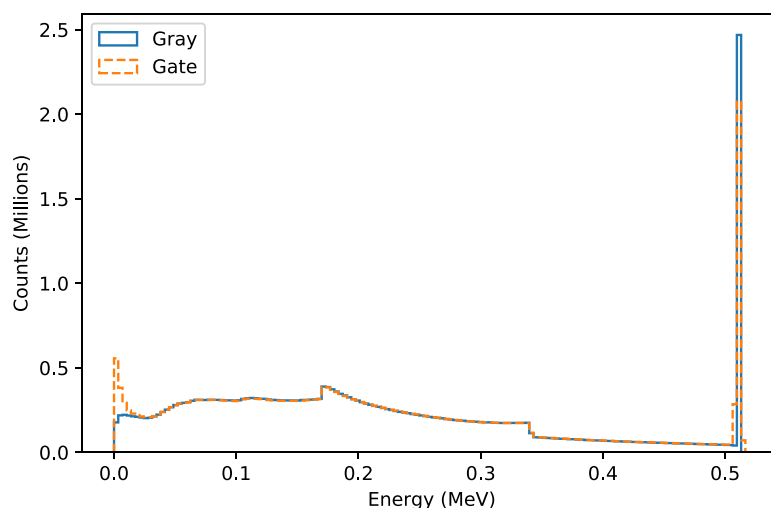


Figure 7. The energy deposited by the hits in the GATE PET Benchmark simulation, as calculated by the two software packages.

When we ran Gray with multiple threads, we see the speedup relative to using a single thread in figure 10. At 8 threads, we see a relative speed up of  $3.975 \pm 0.003 \times$  from the single thread case. Gray in this case was run on macOS High Sierra, and not in a virtual machine to avoid the associated overhead. Running the PET Benchmark in GATE with the positron sources replaced by geantino sources required 72.4% of the original runtime.

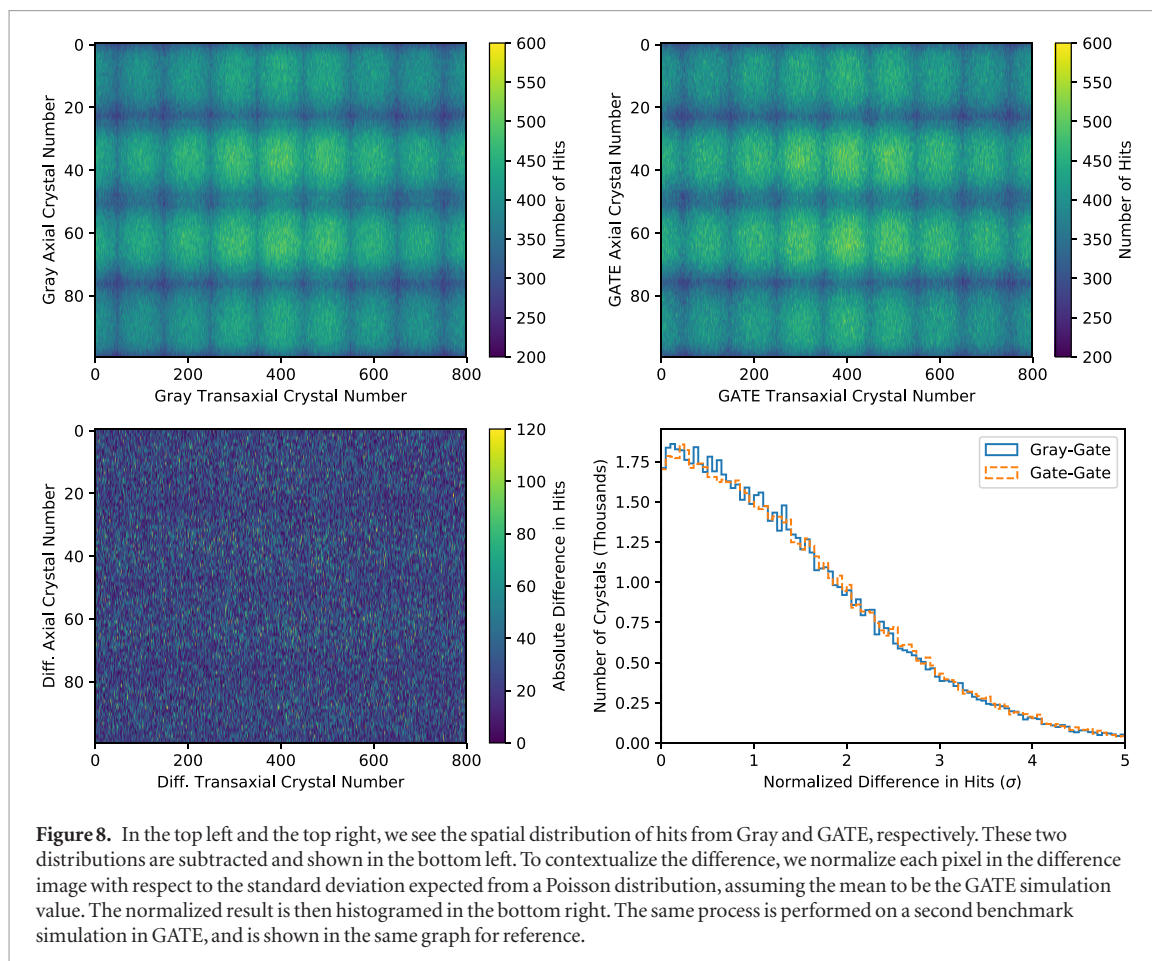
The qualified singles rate for the Siemens Biograph mCT for the varying activity concentrations with the NEMA scatter phantom is shown in figure 11.

The NEMA count rate curves for randoms, trues and scatter, NECR, and scatter fraction are shown in figures 12–15. Table 1 summarizes the average percent difference for the simulated curves as compared to the experimental results presented by Poon *et al*. The last point is excluded as an outlier due to system saturation, as discussed by Poon *et al*. We estimate a peak NECR of  $199.5 \pm 0.2$  kcps at an activity concentration of  $26.9$  kcps  $\text{ml}^{-1}$ , compared to 200 kcps at an activity concentration of  $26.5$  kcps  $\text{ml}^{-1}$  determined experimentally by Poon *et al* (2012).

The axial sensitivity profile calculated from the NEMA sensitivity phantom simulation is shown in figure 16. We calculate a total system sensitivity of  $11.2 \pm 0.1$  cps  $\text{kBq}^{-1}$ . This is a  $14 \pm 3\%$  difference from the  $9.7 \pm 0.2$  cps  $\text{kBq}^{-1}$  by Jakoby *et al*. If we scale the result reported by Jakoby *et al* by the differences in peak NECR to  $10.8 \pm 0.2$  cps  $\text{kBq}^{-1}$  the percent difference becomes  $3 \pm 2\%$ .

#### 4. Discussion

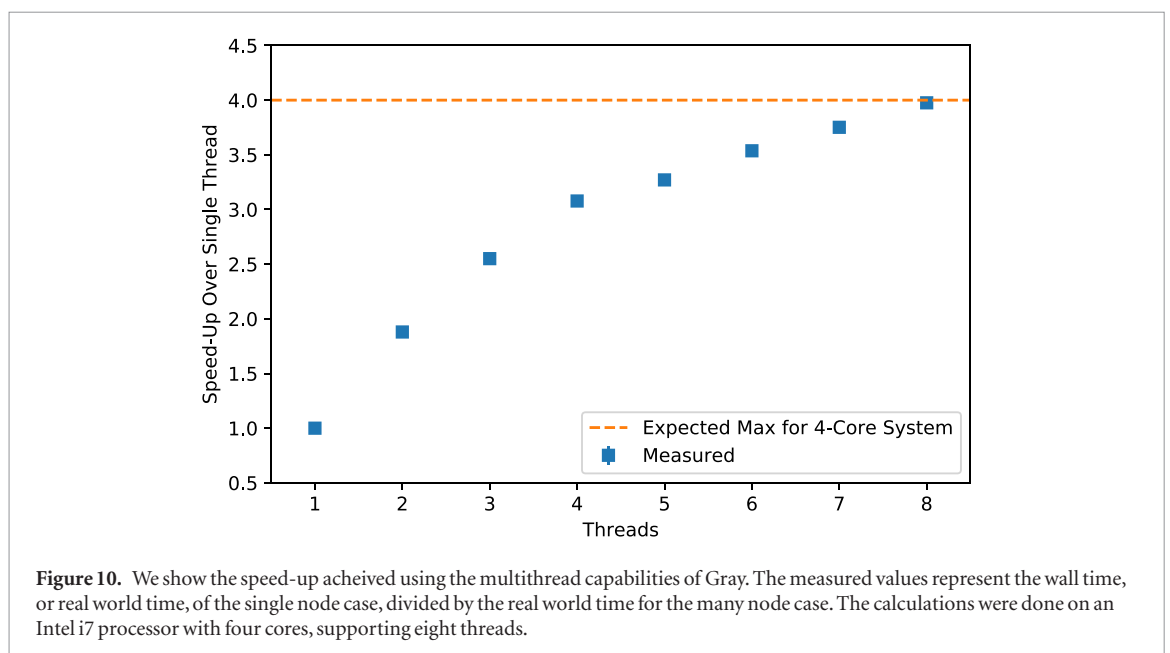
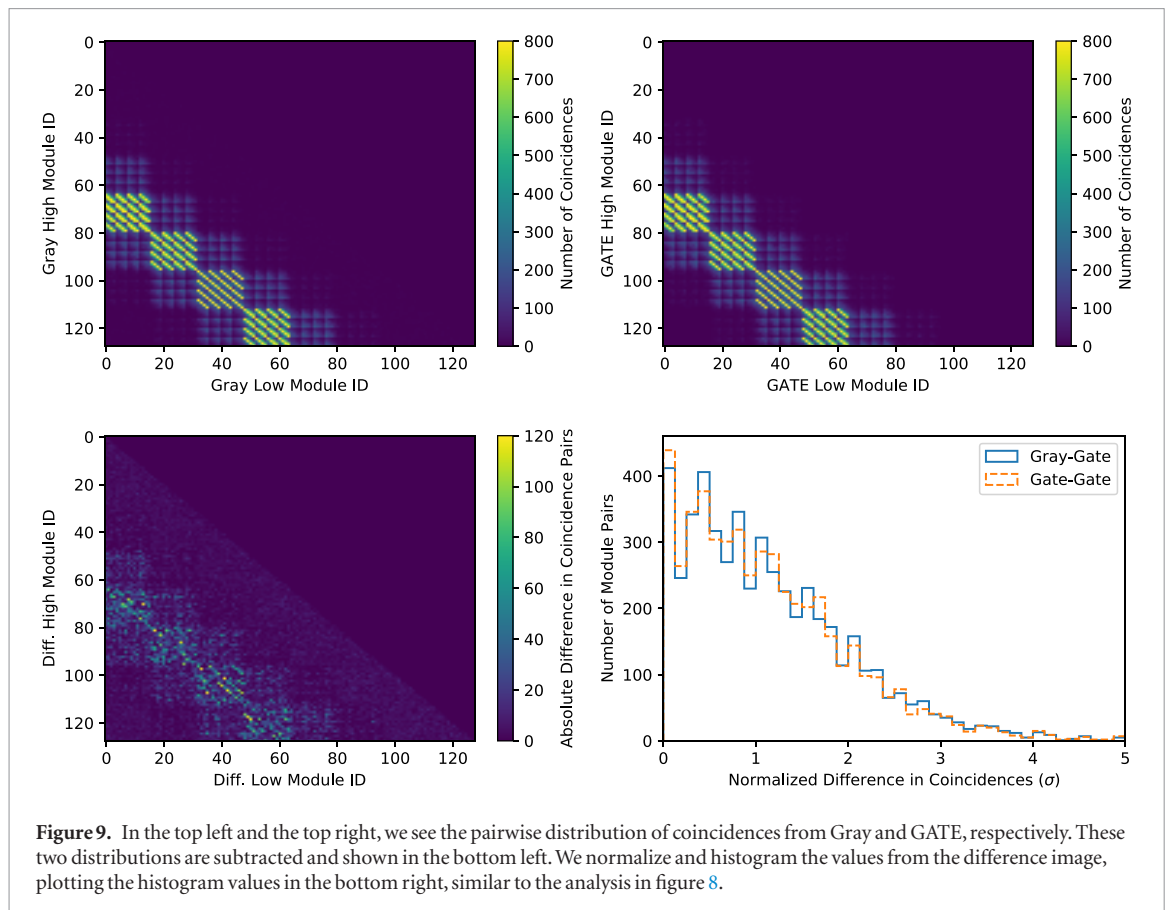
We can see from figures 3–6 that positron range, photoelectric absorption, Compton scattering, Rayleigh scattering have been implemented in Gray accurately within the ray tracing framework. Furthermore, when we



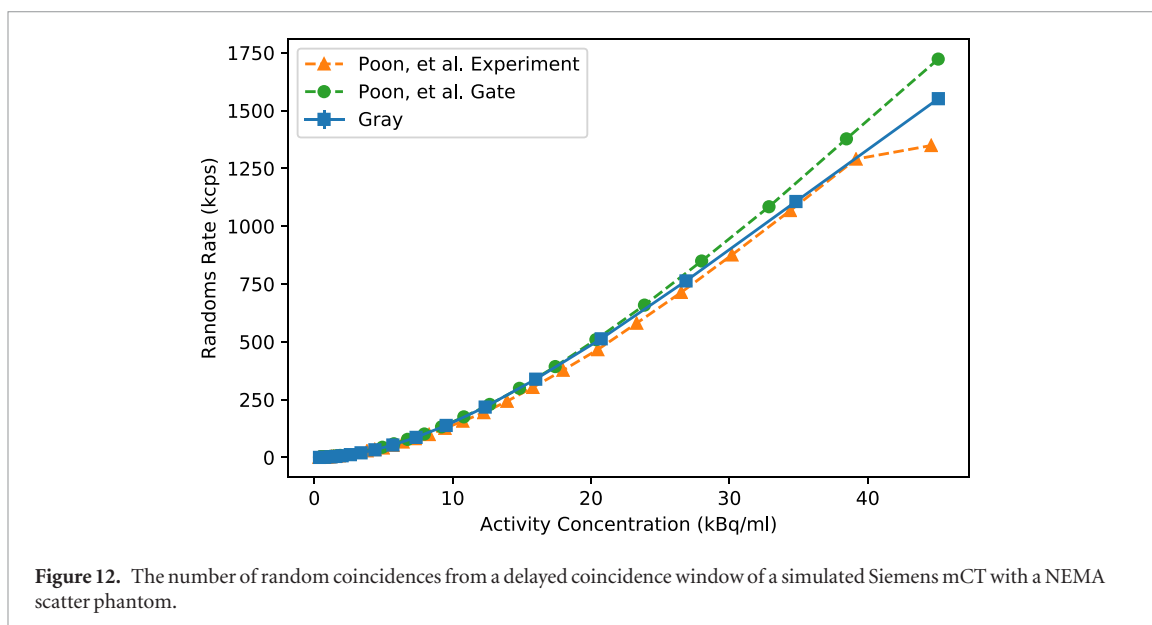
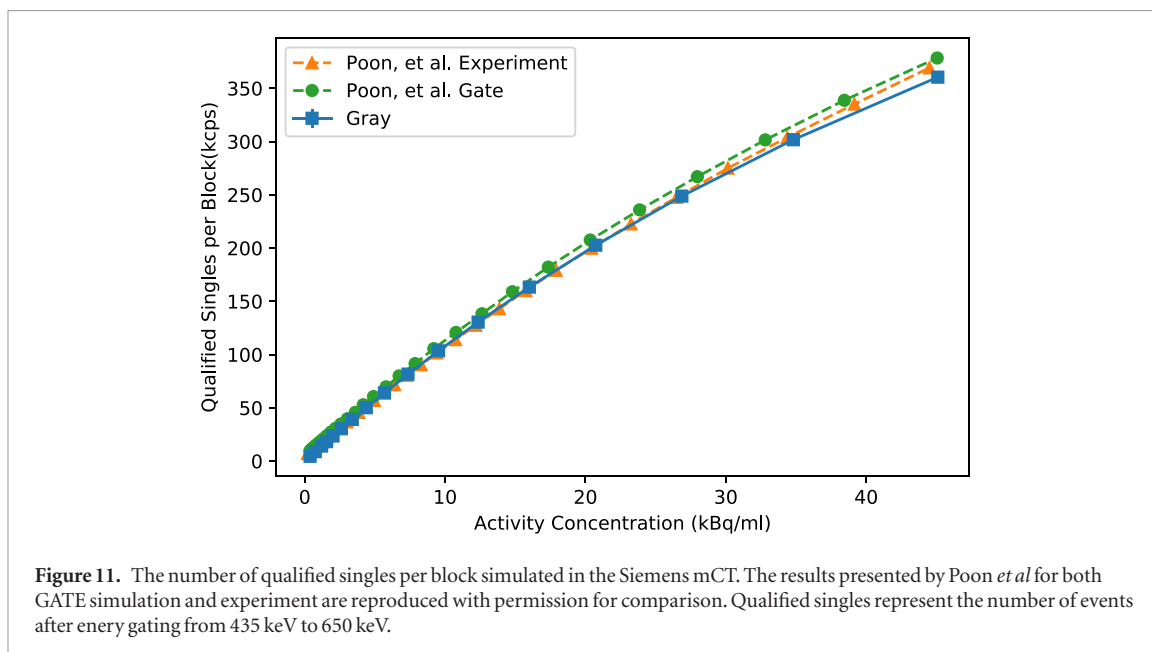
simulate the GATE PET benchmark, we see a  $13.6 \pm 0.1 \times$  speedup in computational time, while still maintaining physical accuracy within what would be expected from statistical error. We can conclude from the fact that GATE takes 72.4% of its total runtime to track particles that do not interact that Gray's primary advantage over GATE is its computational efficiency in tracking photons through the simulation using the k-d tree-based ray tracing backend.

There are some differences in the results of the simulations that can be seen in figure 7 through figure 9. The first obvious difference can be seen at the near zero tail of the energy spectrum in figure 7. This difference is almost entirely attributable to GATE modeling the scattering of electrons within materials. Disabling the 'eMultipleScattering' and 'Bremsstrahlung' physics models in GATE largely removes this difference. Removing these effects results in a 10.2% reduction in runtime for GATE. The speedup for Gray in this case is reduced to  $12.2 \pm 0.1 \times$ . A slight difference at the photopeak in the energy spectrum is also seen in figure 7. Gray neglects that positrons do not annihilate at rest, which causes a small blur in the energies of the emitted gammas from 511 keV. The difference in counts is less than 1.0% if all counts above 508 keV are totaled. As this effect will typically be dominated by the energy resolution of a detector material, we regard this difference as insignificant. For both the hits and the coincidences shown in figures 8 and 9, we see strong agreement between the normalized differences for the Gray-GATE comparison and the GATE-GATE comparison, indicating the differences seen between Gray and GATE are dominated by statistical noise rather than different physics.

The multithread capabilities within Gray, as seen in figure 10 show a good ability to use the full functionality of multicore systems. We achieve almost exactly a  $4 \times$  speed up that we would expect on a quad-core processor for a CPU-bound process. We suspect the fact that this happens at 8 threads, rather than at 4 threads is due to contention with windowing system and other background processes. The Intel Core i7 used for this measurement supports hyperthreading, and thus 8 simultaneous threads. This should not be an issue in more computational environments. Furthermore, Gray is able to automatically detect the number of threads that can be simultaneously run by a machine, allowing it to easily take full advantage of the computational power of the processor. Gray has also been designed to be able to report how it would split a simulation in time over a number of threads. This can be used to equally split the computational load of a simulation over an arbitrary number of nodes within a server cluster, for example. Beyond scaling across many cores and many nodes, we imagine further acceleration of the k-d tree structure should be possible using GPUs (Foley and Sugerma 2005).



For the simulated results of the Siemens Biograph mCT, we see from figure 11 a close match between our results and the experimental results indicating the physical behavior of the Siemens mCT is modeled accurately. Furthermore, this validates our approximation of assuming a continuous, rather than discrete, dead time model. From figures 12–15 we can see that we achieve very good agreement with the experimental results shown by Poon *et al* across all count rates for the NEMA scatter phantom count rate experiment. Particularly we estimate a peak NECR within  $0.5 \pm 0.1\%$  of the experimental peak determined by Poon *et al*, and the activity concentration of the peak within 1.3%. These estimates could potentially be improved by simulating more than 17 activity concentrations. Of key interest is how well Gray matches the experimental curve in figure 14 near the NECR peak. This shows that Gray will be quite useful for simulation studies attempting to optimize peak NECR across different system configurations. The two key differences seen in table 1 are seen in the average percent differences for the qualified singles rate and the randoms rate. The average is increased by larger differences at low activity



levels as Gray does not currently model the  $^{176}\text{Lu}$  background of the scanner. Poon *et al* noted that the  $^{176}\text{Lu}$  background adds 1.1 Mcps in qualified singles. This is equivalent to 5.7 kcps in qualified singles per block, and 1.24 kcps in total randoms coincidences. If we assume we can add a constant to the singles count rate and randoms rate curves to model the additional background, the percent differences for the singles and randoms rates drop to  $11.05 \pm 0.01\%$  and  $11.5 \pm 0.2\%$ , respectively. We anticipate that this background could be readily modeled by a noise process in the Gray DAQ model, as was done by Poon *et al* (2015) in the custom DAQ model used with SimSET without significant impact on runtime.

From figure 16 we see that we accurately reproduce the previously reported axial sensitivity profile up to a scale factor (Jakoby *et al* 2011). The fact that the difference between the scaled total sensitivity from Jakoby *et al* and that reported by Gray are within  $3 \pm 2\%$  shows that Gray appropriately models the physics of the scanner. It is outside the scope of this work to attempt to explain the differences in peak NECR between Poon *et al* and Jakoby *et al*.

The  $13.6 \pm 0.1\times$  speedup we demonstrate here is on the same order of magnitude speed up over GATE noted for SimSET by Poon *et al* (2015). In that work, though, the authors noted several disadvantages for SimSET which are noted: restrictions on the activity distribution with respect to the detectors and the lack of an integrated DAQ model. Gray does not suffer from these limitations, which makes it of particular use for simulation of breast-dedicated systems and other extremity-focus scanners since source geometries can arbitrarily be mixed with detector geometries. Unlike SimSET, though, its runtime is proportional to the simulated number of photons, rather than the detected number of photons, making it less advantageous for simulations with complex geometries in non-sensitive areas of the system. An additional disadvantage of Gray is that the positron range model is fixed to

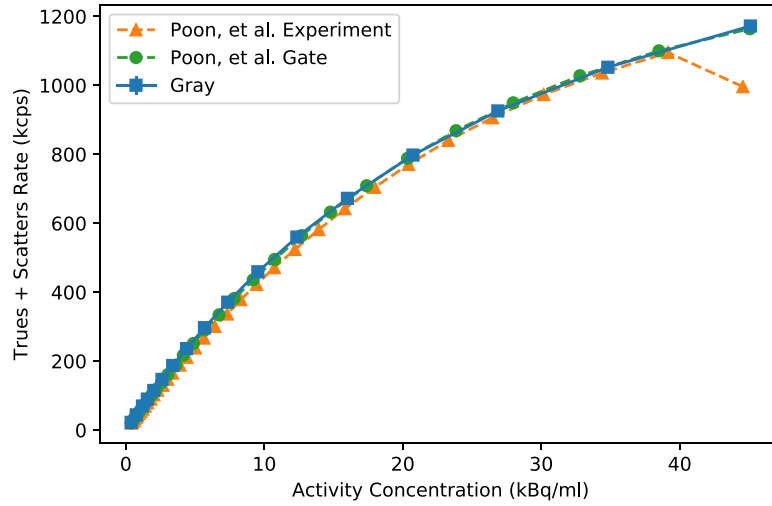


**Figure 13.** The number of true and scattered coincidences simulated in the Siemens mCT using the NEMA scatter phantom. Both prompts and randoms are limited to a 24 cm field of view per the NEMA standard.

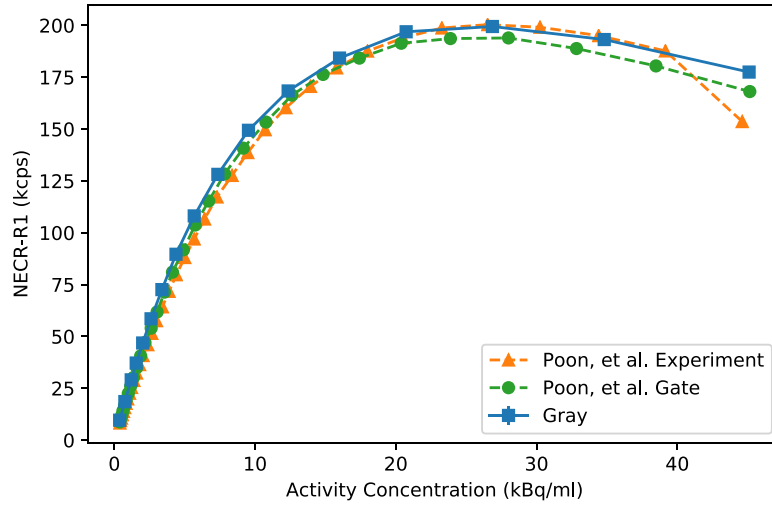


**Figure 14.** The NECR simulated in the Siemens Biograph mCT. A smoothed randoms estimate is assumed to match Poon *et al*.

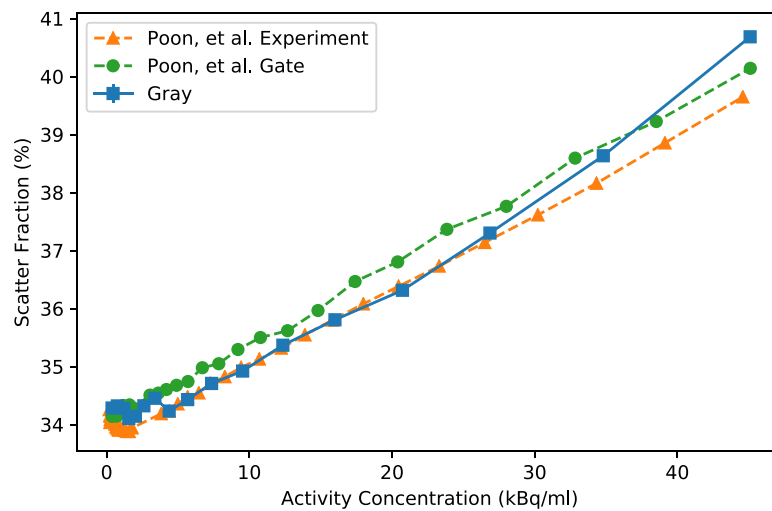
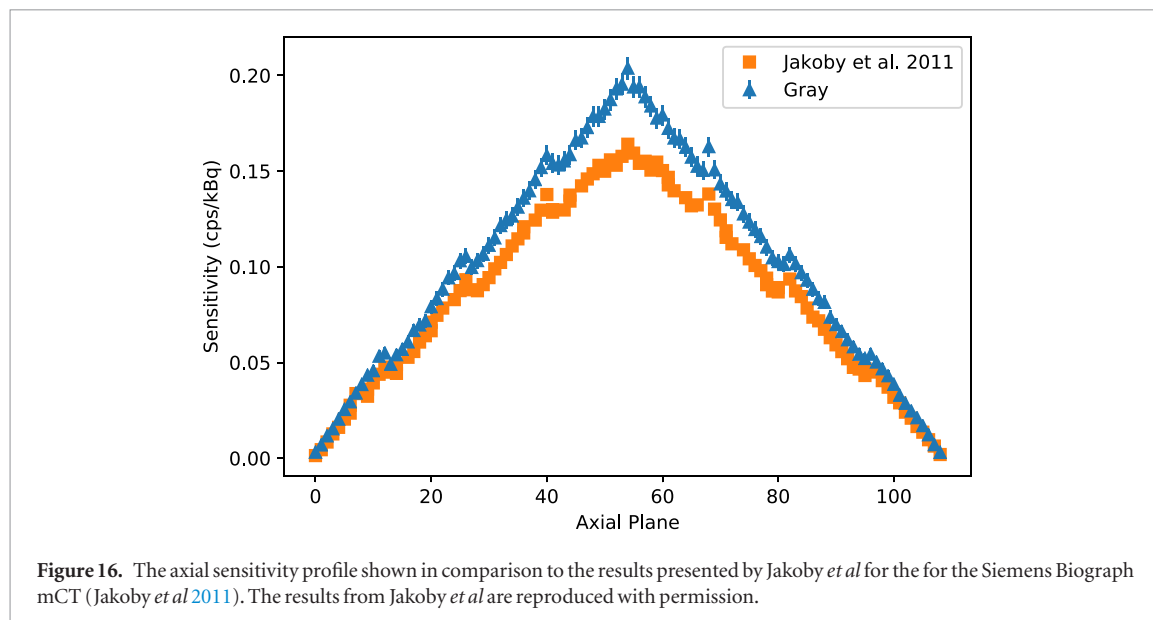


**Figure 15.** The scatter fraction simulated for the Siemens Biograph mCT.

**Table 1.** The average percent difference across all of the NEMA count rate curves compared to the experimental results shown in Poon *et al* (2012). Randoms, Trues and Scatters, and NECR exclude the highest point from their calculations as an outlier due to system saturation.

Type	Gray (%)	Poon <i>et al</i> (%)
Singles	$15.42 \pm 0.01$	9.6
Randoms	$22.8 \pm 0.2$	15.0
Trues and scatters	$10.4 \pm 0.2$	6.3
NECR	$5.5 \pm 0.1$	5.5
Scatter fraction	$0.5 \pm 0.2$	0.8



a reference material, typically water. It does not take into account the material in which the positron is currently located. This can cause inaccuracies inside of less dense material, such as bone or lung, or in the transition into these materials. Gray internally uses the same ray tracing capabilities for photons to track a positron's entry and exit out of a material. We plan to modify this tracking to take into account the different material properties, similar to Harrison *et al* (1999) with SimSET, in the future.

## 5. Conclusion

In this work we introduced Gray, which is a ray-tracing-based Monte Carlo simulator for PET. The ray tracing formulation has several advantages. The primary advantage of ray-tracing is that it is computationally efficient when traversing the scene geometry, and secondly it allows for complex, vectorized geometries of both sources and detectors. We demonstrate correct implementation of several key models in system design for PET: positron range, annihilation acolinearity, photoelectric absorption, Compton scatter, and Rayleigh scatter. We see an  $13.6 \pm 0.1 \times$  speedup using Gray, compared to GATE, and achieve statistically similar results when simulating the GATE PET benchmark. We show that both the physics and DAQ model implemented allow accurate modeling of the NEMA sensitivity and count rate performance of the Siemens Biograph mCT, estimating the sensitivity within  $3 \pm 2\%$ , and the peak NECR within  $0.5 \pm 0.1\%$ .

## Acknowledgments

The authors would like to thank Jonathan Poon, Edwin Leung, and Ramsey Badawi from the University of California, Davis for providing the GATE geometry description of the Siemens Biograph mCT used in their previous work as well as their time in answering the authors' questions. Their help in replicating their work with Gray proved invaluable for providing an experimental validation of Gray. The authors would also like to thank Garry Chinn for helpful discussions regarding the data acquisition model.

## ORCID iDs

David L Freese  <https://orcid.org/0000-0001-6954-1292>



## References

- Aklan B, Jakoby B W, Watson C C, Braun H, Ritt P and Quick H H 2015 Gate Monte Carlo simulations for variations of an integrated PET/MR hybrid imaging system based on the biograph MMR model *Phys. Med. Biol.* **60** 4731
- Buss R S 2003 *3D Computer Graphics: a Mathematical Introduction with OpenGL* (Cambridge: Cambridge University Press)
- Cullen D E, Hubbell J H and Kissel L 1997 *EPDL97: the Evaluated Photon Data Library (UCRL-50400 vol 6)* (Washington, DC: Department of Energy) pp 1–28
- DeBenedetti S and Siegel R T 1954 The three-photon annihilation of positrons and electrons *Phys. Rev.* **94** 955–9
- Delso G, Fürst S, Jakoby B, Ladebeck R, Ganter C, Nekolla S G, Schwaiger M and Ziegler S I 2011 Performance measurements of the siemens MMR integrated whole-body PET/MR scanner *J. Nucl. Med.* **52** 1914–22
- Derenzo S 1979 Precision measurement of annihilation point spread distributions for medically important positron emitters *Positron Annihilation* ed R R Hasiguti and K Fujiwara (Sendai: The Japan Institute of Metals) pp 819–23
- Foley T and Sugerman J 2005 KD-tree acceleration structures for a GPU raytracer *Proc. of the ACM SIGGRAPH/EUROGRAPHICS Conf. on Graphics Hardware* (New York: ACM) pp 15–22
- Gonias P et al 2007 Validation of a GATE model for the simulation of the siemens biograph<sup>TM</sup>6 PET scanner *Nucl. Instrum. Methods Phys. Res. A* **571** 263–6
- Guez D, Bataille F, Comtat C, Honore P F, Jan S and Kerhoas S 2008 Counting rates modeling for PET scanners with GATE *IEEE Trans. Nucl. Sci.* **55** 516–23
- Harrison R L, Gillispie S B and Lewellen T K 2006 Design and implementation of a block detector simulation in SimSET *IEEE Nuclear Science Symp. Conf. Record* vol 5 pp 3151–3
- Harrison R L, Kaplan M S, Vannoy S D and Lewellen T K 1999 Positron range and coincidence non-collinearity in SimSET *IEEE Nuclear Science Symp. Conf. Record. 1999 Nuclear Science Symp. and Medical Imaging Conf. (Cat. No.99CH37019)* vol 3 pp 1265–8
- Harrison R L, Vannoy S D, Haynor D R, Gillispie S B, Kaplan M S and Lewellen T K 1993 Preliminary experience with the photon history generator module of a public-domain simulation system for emission tomography *IEEE Conf. Record Nuclear Science Symp. and Medical Imaging Conf.* pp 1154–8
- Jakoby B W, Bercier Y, Conti M, Casey M E, Bendriem B and Townsend D W 2011 Physical and clinical performance of the MCT time-of-flight PET/CT scanner *Phys. Med. Biol.* **56** 2375
- Jan S et al 2011 GATE v6: a major enhancement of the GATE simulation platform enabling modelling of CT and radiotherapy *Phys. Med. Biol.* **56** 881
- Kaplan M S, Harrison R L and Vannoy S D 1998 Coherent scatter implementation for simset *IEEE Trans. Nucl. Sci.* **45** 3064–8
- Lamare F, Turzo A, Bizais Y, Rest C L C and Visvikis D 2006 Validation of a Monte Carlo simulation of the philips allegro/gemini PET systems using GATE *Phys. Med. Biol.* **51** 943
- Levin C S and Hoffman E J 1999 Calculation of positron range and its effect on the fundamental limit of positron emission tomography system spatial resolution *Phys. Med. Biol.* **44** 781
- MacDonald L R, Schmitz R E, Alessio A M, Wollenweber S D, Stearns C W, Ganin A, Harrison R L, Lewellen T K and Kinahan P E 2008 Measured count-rate performance of the discovery STE PET/CT scanner in 2d, 3d and partial collimation acquisition modes *Phys. Med. Biol.* **53** 3723
- Ore A and Powell J L 1949 Three-photon annihilation of an electron–positron pair *Phys. Rev.* **75** 1696–9
- Poon J K, Dahlbom M L, Casey M E, Qi J, Cherry S R and Badawi R D 2015 Validation of the SimSET simulation package for modeling the siemens biograph mct pet scanner *Phys. Med. Biol.* **60** N35
- Poon J K, Dahlbom M L, Moses W W, Balakrishnan K, Wang W, Cherry S R and Badawi R D 2012 Optimal whole-body PET scanner configurations for different volumes of LSO scintillator: a simulation study *Phys. Med. Biol.* **57** 4077
- Schmidtlein C R et al 2006 Validation of gate Monte Carlo simulations of the ge advance/discovery LS PET scanners *Med. Phys.* **33** 198–208
- Shibuya K, Yoshida E, Nishikido F, Suzuki T, Tsuda T, Inadama N, Yamaya T and Murayama H 2007 Annihilation photon acollinearity in PET: volunteer and phantom FDG studies *Phys. Med. Biol.* **52** 5249